Accepted Manuscript

Effect of the filament discharge current on the microstructure and performance of plasma-enhanced magnetron sputtered TiN coatings

Xin Zhang, Yan-Wen Zhou, Jian-Bo Gao, Zhi-Wei Zhao, Yuan-Yuan Guo, Zhi-Wen Xie, Peter Kelly

Please cite this article as: X. Zhang, Y.-W. Zhou, J.-B. Gao, Z.-W. Zhao, Y.-Y. Guo, Z.-W. Xie, P. Kelly, Effect of the filament discharge current on the microstructure and performance of plasma-enhanced magnetron sputtered TiN coatings, *Journal of Alloys and Compounds* (2017), doi: 10.1016/j.jallcom.2017.05.037.

Effect of the filament discharge current on the microstructure and performance of plasma-enhanced magnetron sputtered TiN coatings

Xin Zhang[1], Yan-Wen Zhou*[1], Jian-Bo Gao[1], Zhi-Wei Zhao[1], Yuan-Yuan Guo[1],

Zhi-Wen Xie[1], Peter Kelly**[2]

[1]Surface Engineering Institute, University of Science and Technology Liaoning

[2]Surface Engineering Group, Manchester Metropolitan University

Abstract: Titanium nitride (TiN) coatings were synthesized by plasma-enhanced magnetron sputtering (PEMS) on 316L austenitic stainless steel and YG8 cemented carbide substrates. The plasma enhancement process involved the use of hot filaments as additional sources of electrons for the magnetron discharge. The structural, morphology, crystallinity, thickness, abrasion resistance and adhesion of the TiN coatings, as well as the nanohardness and Young's modulus were investigated at different filament discharge currents. The results showed that with increasing discharge current, the deposition rate of the coating decreased, the structural morphology of the TiN coatings became finer and denser and the columnar grain size decreased. The critical load for failure in scratch adhesion tests of the coatings on stainless steel and YG8 substrates were over 22 N and 141 N, respectively. The nanohardness and Young's modulus both improved significantly from 8 GPa and 200 GPa to 38 GPa and 500 GPa, respectively, after the discharge current increased from 6 A up to 12 A. The adhesion and the abrasion resistance of the coating on cemented

carbide increased, and those on stainless steel decreased, with increasing filament discharge current. It was found that matching the Young's modulus of the coating to that of the substrate was important to improve the adhesion and abrasion resistance of the coating. The results demonstrate that TiN coatings can be prepared by PEMS at appropriate filament discharge currents, resulting in coatings with uniform thickness, dense structure and high hardness, abrasion resistance and adhesion.

Key words: plasma-enhanced magnetron sputtering; TiN coatings; filament discharge current; microstructure; performance

1 Introduction

It is well established that the physical and chemical properties of physical vapor deposition (PVD) coatings are strongly influenced by the coating microstructure [1] . Properties, such as hardness, wear resistance, abrasion resistance, corrosion resistance, etc. have been shown to be determined, at least in part, by the microstructure. However, the microstructure is, in turn, determined by a number of deposition and process parameters, including substrate temperature, coating pressure, substrate bias voltage and the ion-to-atom ratio incident at the substrate. All of these parameters affect the energy delivered to the growing film. This energy controls the mobility of the deposited atoms and is, therefore, the critical factor in determining the final coating microstructure. In the field of magnetron sputtering, historical developments, such as unbalanced magnetrons, closed field unbalanced sputtering (CFUBMS) and

pulsed magnetron sputtering [2] have all influenced the energy delivered to the growing films and, through this, made step-changes in the performances of coatings deposited by these techniques. More recently, high power impulse magnetron sputtering (HiPIMS) has been promoted as another means of increasing the ion-to-atom ratio and producing coatings with enhanced properties. However, HiPIMS is also associated with low deposition rates and is a technique that cannot be readily introduced into a conventional CFUBMS coating system. Where the major rig modifications required for HiPIMS mode are not an option, an alternative approach demonstrated here, is the use of hot filaments to boost the degree of ionisation in the chamber and, thereby, provide a means of controlling film properties, using a simple DC current supply.

The plasma-enhanced magnetron sputtering (PEMS) technique [3] used in this study is based on traditional balanced magnetron sputtering, with additional tungsten filaments installed that can act as electron emission sources in the vacuum chamber in order to create additional process gas ionisation and improve the plasma density. The amount of electrons emitted from the filaments is described in terms of the 'filament discharge current' delivered from a DC current supply. The chamber has four balanced magnetrons, and four filaments are fitted between the targets. These filaments extend to the full height of the chamber and, therefore, provide uniform ion bombardment across the substrate holder. This technique has been shown to be capable of delivering coatings with enhanced structures, hardness, better toughness

and adhesion onto batches of industrial workpieces [4], without the need for expensive and complex power delivery modes.

To further investigate the technique, titanium nitride (TiN) coatings have been deposited onto stainless steel and WC/Co cemented carbide substrates. TiN is a widely used industrial coating material, with high strength, good corrosion resistance [5-10] etc. The structure and properties of TiN coatings are very sensitive to the nitrogen flux under different reactive sputtering conditions [6, 7]. It is often deposited onto stainless steel [5, 9], high-speed steel, carbide and mould steels which are applied to tools, moulds and mechanical parts, MEMS [11] and other fields. The wear resistance is the main property for many practical applications, such as olive oil extraction [5, 9]. The properties can be modified by surface texture control [6, 8]. Stainless steel is widely used in chemical, petroleum, medical, aerospace applications, as well as in marine engineering, decorative engineering etc., because of its high corrosion resistance [5, 12-14]. However, the hardness of stainless steel is usually low and, its wear resistance is poor, thus limiting its use in certain environments [15, 16]. The surface treatment of stainless steel can significantly improve its wear and corrosion resistance. WC/Co cemented carbide has been applied on cutting tools, engine components subject to wear, spray nozzles and other mechanical components due to its high hardness, corrosion resistance and high temperature resistance [6, 17-19]. Nevertheless, the surface hardness of the WC/Co cemented carbide substrate is able to be further enhanced by nitride coatings, while at the same time, retaining the toughness of the bulk substrate.

In this study, therefore, TiN coatings were fabricated on 'soft' 316L austenitic stainless steel and 'hard' YG8 cemented carbide substrates by PEMS at different filament discharge currents. The effects of the discharge current on the microstructure and properties of the TiN coatings on the 'hard' and 'soft' substrates were investigated.

2 Experimental

2.1 Materials and Processes

The substrate materials used in these experiments were 316L austenitic stainless steel coupons with a thickness of 5 mm and diameter of 20 mm and, YG8 cemented carbide substrates with a thickness of 5mm and size 20 x 20 mm^2. The surfaces of the samples were mechanically polished to a mirror finish and then ultrasonically cleaned in acetone and absolute ethanol for 30 min. The samples were then dried with nitrogen and placed in the vacuum chamber, which was 900 mm in diameter and 1000 mm in height. There are four balanced magnetrons installed through the chamber walls, each with a 99.9% pure titanium target attached. Each magnetron is driven by a pulsed DC power supply. The power supply was set to 9 A in current regulation mode at a frequency of 50 KHz and duty of 80%. The substrate holder was fully loaded with samples to simulate the batch coating conditions. When the base pressure reached 3×10^{-3} Pa, the chamber was heated up to 350° C. The argon gas was introduced to give a working pressure of 0.4 Pa and the substrates were subjected to plasma cleaning. The bias voltage on the substrates were first set to -120 V for 900 s and then -300 V

for 900 s. Then after depositing a Ti interlayer for 300 s, nitrogen gas was introduced progressively up to a flow rate of 65 sccm over 120 s to give a graded Ti/TiN interface. TiN coatings were then deposited at a substrate bias of -50 V for 5 h. To prepare the tungsten filaments, three tungsten wires of 0.4 mm diameter and length 1000 mm were twinned together to make one filament and four filaments were installed in the chamber. The filaments were connected to a 50Hz AC power to heat the electrons of the filament, and biased at -120 V by a DC power supply which is isolated with the AC power. To obtain the required discharge currents from the filaments, the currents from the AC powers were adjusted. The specific experimental process parameters are shown in Table 1.

2.2 Characterization of coatings

Selected substrates were partially masked to produce a step in the coating, which was used to measure the thickness of the coatings using an Alpha-step D-100 type stepper and, the average deposition rate was calculated from these thickness measurements. The phase structure of the TiN coating was analyzed by X'Pert Powder X-ray diffractometer in a $\theta \sim 2\theta$ scanning mode from 20 to 90° for 480 s. The surface and cross-sectional morphology of the coating were observed by SIGMA HD field emission scanning electron microscopy, and the composition by EDS. The friction and wear properties of the coatings were measured using a MS-T3001 friction and wear tester. The rotational speed was 3.33 r/s, the load was 400 g and the test time was 3600 s. The friction coefficient was measured throughout the whole wear test process.

The wear profile was then measured by using an Alpha-step D-100 type stepper and the wear resistance was compared from the profile. The adhesion force between the coating and the substrate was measured by a MFT-4000 scratch tester. A Rockwell indenter with radius of 0.2 mm and pressure angle of 120 $^{\circ}$ was used in the scratch test, where the load was increased progressively up to a final load of 100 N over a scratch length of 5 mm. The critical load was determined by the first failure chip detected by acoustic emissions. A standard Berkovich indenter was used to determine the nano-hardness and Young's modulus using a G200 nano-hardness tester. The load displacement was set to 1000 nm, and an average of 20 test points was measured.

3 Results and discussion

3.1 Substrate ion density

The ion currents on substrate were measured by changing substrate bias voltage at different filament discharge currents and, from which the substrate current densities were calculated, shown in Figure 1. Without using the filaments, the substrate currents were almost equal to zero because the plasma was confined in front of targets by the balance magnetrons. It implied that there were hardly ions arrived to the substrate even if the substrate bias voltage increased to 100 V. The substrate current density increased significantly by using the filaments. The current density was 6.5 x 10^{-3} mA/mm^2 at bias voltage of 100 V when one filament discharge current was set to 6 A. It increased to 10 x 10^{-3} mA/mm^2 and 12.5 x 10^{-3} mA/mm^2 when one filament discharge current was 9 A and 12 A, respectively. The current densities on substrate

grew to double with doubling filament discharge current, i.e. the ionization rate doubled. On the other hand, the current density increased slowly as the increase of the substrate bias voltage. Therefore, the filament discharge current provides the ion flux to the substrate, whilst the bias voltage provides the energy to ions.

3.2 Deposition rate and microscopic morphology

The deposition rates of the TiN coatings at different tungsten filament discharge currents are shown in figure 2. With increasing discharge current, the apparent deposition rates of the TiN coatings decreased continuously. However, the deposition rates were calculated from coating thickness values and do not take into account variations in film structure and density. It is clear that increasing the filament discharge current increases the flux of emitted electrons into the chamber and therefore, results in the increased ionization rates of Ar and N_2. This will lead to increased ion bombardment of the growing film, causing resputtering and film densification. Thus it is also necessary to consider variations in film structure as a function of filament current.

The surface and sectional morphology of TiN coatings prepared at different discharge currents are shown in Figures 3a, 3b and 3c. The surface morphology changed from loose triangles of the coating deposited at discharge current of 6 A, to denser equiaxed shaped grains for the coatings at 9 A, and then a fully dense structure at 12 A. Fracture sections of the TiN coatings indicated that they grew with columnar structures and the compactness of the columns increased with increasing filament

discharge current. As shown in Figures 3a and 3b, the columns of the coating deposited at a discharge current of 6 A were loose and thick, while those at 9 A were closer and finer. The fracture morphology of the columns at 12 A in Figure 3c was even more compact, which implied that high compressive stresses remained in the coatings due to the increased flux of ions at the substrate. The dense and fine columnar structure of the TiN coatings would be expected to result in improvements of the wear and corrosion resistances [9]. On the other hand, the high stress within the coating may decrease the adhesion of the coating to substrate and cause delamination.

Figure 4 shows high resolution TEM micrographs of the TiN coating deposited at a discharge current of 12 A. In Figure 4a, the dense nano-columns were visible and the diffraction spots were bright and clear in the selected area electron diffraction (SAED) pattern, shown in Figure 4b, indicating that that this coating was crystalline. The high resolution image shown in Figure 4c and, of which the SAED pattern in Figure 4d, indicated deformation of the TiN lattice due to the increased ion bombardment. As also shown in Figure 4, W was detected in the TiN coating. The W came from the hot W filaments, which were negatively biased and, therefore, also subject to ion bombardment during the whole deposition process.

3.3 Composition and crystal structure

Changes in the atomic ratio of N and Ti and the W content in TiN coatings at different discharge currents are shown in Figure 5. The ratio of N and Ti atoms decreased and the W content increased with increasing filament discharge current.

The nitrogen flow rate was kept constant for all deposition runs. However, as discussed in section 3.1, increasing the filament discharge current increased the plasma density in the chamber, which presumably led to greater bombardment and higher sputtering rates at the Ti targets, thus increasing the Ti content of the films, relative to the N content.

The increasing discharge current also meant that more electrons were emitted from the W filaments and that the filaments became hotter. This may result in evaporation of W from the filaments, but again, the increased plasma density in their vicinity would also lead to greater sputtering of the filaments.

Figure 6 shows the XRD patterns of the TiN coatings. Because TiN is a face-centered cubic lattice structure with a close-packed (111) surface, little energy was required for the growth of TiN on this surface, and so the preferred orientation of TiN was (111). It can be seen from the figure that the preferred orientations of TiN coatings along the (111) and (222) directions were less obvious with increasing discharge current, implying that the crystallinity of TiN decreased with increasing discharge current. The (111) diffraction peak of the TiN coatings was also associated with the WN (111) peak, indicating that W atoms from the filaments combined with the nitrogen. As discussed in Figures 4c and 4d in section 3.2, the deformation of the TiN lattice was due to the coexistence of the WN phase and the intensive ion bombardment with increasing filament discharge current. Other studies [8, 20] have concluded that the implantation of W ions reduces grain size and increases compressive stress. The crystallite size of the TiN coatings, calculated according to

the Scherrer formula, is given in Table 2. The crystallite size decreased with increasing filament discharge current by greater than a factor of 4 as the current is increased from 6 A to 12 A. The difference in this study was the formation of a WN phase instead of the implantation of W ions, however the results agree with the conclusion above.

3.4 Mechanical properties of the TiN coatings

The nano-hardness (H) and Young's modulus (E), H/E and H^3/E^2 of the 316L and YG8 substrates and, the TiN coatings at different filament discharge currents are shown in Table 2. The nano-hardness and Young's modulus related to the displacement into the surface of the substrates and the TiN coatings were shown in Figures 7a and 7b, respectively. The ratio of H/E is related to the material's elastic strain limit, which characterizes the ability of the material to deform elastically and recover [10, 21]. The ratio of H^3/E^2 indicates the resistance of materials to plastic deformation [22]. The nano-hardness and Young 's modulus increased significantly as the filament discharge current increased from 6 A to 9 A, but then remained at approximately the same values at 12 A. H/E and H^3/E^2 showed the same trends as nano-hardness and Young's modulus.

The increased hardness of the coating was due to the increased degree of ion bombardment on the growing coating as the discharge current increased from 6 A to 9 A [6]. However, the hardness and modulus of the TiN coating prepared at discharge currents of 9 A and 12 A reached its limit, i.e. 35-38 GPa and 450-500 GPa,

respectively. Further increasing the flux of ions did not have a measurable effect on the hardness and modulus of the TiN coating.

The adhesion of the TiN coating at different discharge currents is also shown in Table 2. The acoustic emission signal to the load on the TiN coatings on 316L and YG8 substrates are shown in Figures 8a and 8b, respectively. With increasing discharge current, the adhesion of TiN coating on 316L stainless steel decreased, that on YG8 increased.

Coatings with high H/E are believed to be tough and, with high H^3/E^2 to be hard. However, the adhesion of the tough and hard TiN coating deposited at 9 A and 12 A on 316L stainless steel and YG8 cemented carbide substrates were about 22 N and 200 N, respectively. The difference of the adhesion of the same coating on 316L steel and YG8 carbide were obvious. The Young's modulus of the two substrate materials is very different and it was believed that the difference of modulus between the coating and substrate was the key factor to determining the adhesion of the coating to substrate. The modulus of YG8 was higher than those of the TiN coatings deposited at 9 A and 12 A, and the adhesion of the coatings to YG8 was so good that it was beyond the limitation of the scratch tester used in this study, refer to Figure 8b. Again, the modulus of stainless steel was a little higher than that of the TiN coating deposited at 6 A, which also showed good adhesion of 87 N.

The Rockwell indentations of the coatings deposited at the current of 12 A are shown in Figures 9a and 9b. There is very little evidence of delamination of the coatings, both on 316 stainless steel and YG8 cemented carbide, around the

circumference of the indentations. Therefore, the toughness of the coating is excellent. The adhesion of the coatings on both substrates is expected to be good, according to the study by Vidakis [23] and the VDI 3198 indentation test evaluation. However, the adhesion of the TiN on 316L deposited at 12 A was only 22 N. The failure of the adhesion occurred due to the difference of elastic deformation and recovery between the coating and the substrate, i.e. the match of the Young's modulus of the coating and substrate was important.

The wear profiles of the TiN coatings at different filament discharge currents on 316L and YG8 substrates are shown in Figures 10a and 10b, and the friction coefficients are listed in Table 2. Although there was no significant change in the friction coefficient, the surface abrasion resistance varied with the change of discharge current.

It was interesting that the wear volume of the TiN coatings on 316L steel were apparently greater with increasing hardness of the coating. Considered the adhesion of TiN coating on 316L, it was possible that the anti-strain ability between the coating and 316L substrate was lower and, the harder coating failed very soon when the friction pair loaded on it. In contrast, the abrasive resistance of the TiN coatings on YG8 cemented carbide was enhanced with increasing discharge current. A study by Ping Chen etc. showed that the tribological performance can be improved due to high hardness and low elastic modulus [10, 23]. However, it is very difficult to improve the hardness and reduce the Young's modulus at the same time. Musil and Leyland and Matthews proposed a hardness to elastic modulus ratio (H/E ratio) as an important

parameter in the wear mechanism [21, 22]. From this study, it is suggested that another parameter is added, Δ E', the difference between a coating and substrate, to evaluate the abrasive resistance. The wear resistance of a coating is able to be improved with high H/E and small Δ E.

4 Conclusions

A series of TiN coatings have been deposited by plasma enhanced reactive magnetron sputtering onto two substrate materials with different mechanical properties. The level of plasma enhancement during the deposition process was controlled by the relatively simple approach of varying the current to tungsten filaments positioned in the coating chamber. With increasing filament discharge current, the deposition rate of TiN coatings decreased, the coatings became denser, the ratio of N/Ti decreased, and the presence of a WN phase within the TiN lattice caused lattice deformation. The nanohardness and Young's modulus increased to about 35 ~38 and 450 ~500 GPa, respectively, whereas the H/E and H^3/E^2 values increased to 0.07 and 0.18~0.19, respectively. The highest adhesion strength of the TiN coating deposited at 6 A on 316L stainless steel was 86 N and, that of the TiN coating deposited at 9 A on YG8 was 200 N. The abrasion resistance of the TiN coating on 316L steel deteriorated and, that of the coating on YG8 carbide improved with increasing filament discharge current and the coating hardness. Minimising the difference in Young's modulus between the coating and substrate was identified as an

important to parameter in improving the adhesion and abrasive resistance of the coating.

Figure captions

Fig. 1 Substrate current density as a function of substrate bias voltage

Fig. 2 Deposition rate of TiN coatings as a function of filament discharge current

Fig. 3 The surface and sectional morphology of TiN coatings at filament discharge currents of (a) 6 A, (b) 9 A and (c) 12 A

Fig. 4 The high resolution images of the TiN coating at 12 A: (a) sectional image, (b) SEAD pattern of the sectional image, (c) high resolution image and (d) SEAD pattern of the high resolution image

Fig. 5 The N/Ti ratio and the W content in TiN coatings as a function of filament discharge current

Fig. 6 XRD patterns of the TiN coatings

Fig. 7 Nano-hardness (a) and Young's modulus (b) as a function of displacement into the surface of the substrates and the TiN coatings

Fig. 8 Acoustic emission signal to the progressive load on the TiN coating: (a) on 316L and (b) YG8 substrates

Fig. 9 Rockwell indentation of the TiN coating at 12 A: (a) on 316L stainless steel and (b) on YG8 cemented carbide

Fig. 10 Wear profile of TiN coatings: (a) on 316L stainless steel and (b) on YG8 cemented carbide

Table Caption

Table 1 Experimental process parameters

Table 2 Performance comparison of TiN coatings on 316L austenitic stainless steel and YG8 cemented carbide

Reference

[1] P.J. Kelly, R.D. Arnell, DEVELOPMENT OF A NOVEL STRUCTURE ZONE MODEL RELATING TO THE CLOSED-FIELD UNBALANCED MAGNETRON SPUTTERING SYSTEM, Journal of Vacuum Science Technology, 16 (1998) 2858-2869.

[2] P.J. Kelly, R.D. Arnell, Magnetron sputtering: a review of recent developments and applications, Vacuum, 56 (2000) 159-172.

[3] C.M. Li, R.H. Wei, Application of Ti(Al) based nanocomposite coatings on cast aluminum molds by plasma enhanced magnetron sputtering, China Surface Engineering, 25 (2012) 1-7.

[4] H. Li, Y. Liu, B. Jiang, J. Kan, Z. Liu, The structure and toughness of TiN coatings prepared by modulated pulsed power magnetron sputtering, Vacuum, 125 (2016) 165-169.

[5] A. Bahri, N. Guermazi, K. Elleuch, M. Ürgen, Tribological performance of TiN coatings deposited on 304 L stainless steel used for olive-oil extraction, Wear, 342–343 (2015) 77-84.

[6] J.W. Cheng, H.Y. Fan, Y.P. Tian, Influence of Nitrogen Flux on Microstructure and Mechanical Properties of TiN Films Deposited by Reactive Magnetron Sputtering, Cemented Carbide, 29 (2012) 203-207.

[7] Y.C. Zhong, X.R. Ren, Z. Huang, Effect of nitrogen flow on microstructure and mechanical properties of TiN films, Nonferrous Metals Science and Engineering, 7 (2016) 47-53.

[8] L.P. Ward, K.P. Purushotham, R.R. Manory, Studies on the surface modification of TiN coatings using MEVVA ion implantation with selected metallic species, Nuclear Instruments and Methods in Physics Research Section B: Beam Interactions with Materials and Atoms, 368 (2016) 37-44.

[9] A. Bahri, E. Kaçar, S.S. Akkaya, K. Elleuch, M. Ürgen, Wear protection potential of TiN coatings for 304 stainless steels used in rotating parts during olive oil extraction, Surface and Coatings Technology, 304 (2016) 560-566.

[10] P. Chen, X. Xiang, T. Shao, Y. La, J. Li, Effect of triangular texture on the tribological performance of die steel with TiN coatings under lubricated sliding condition, Applied Surface Science, 389 (2016) 361-368.

[11] W. Xiang, C. Zhao, K. Liu, G. Zhang, K. Zhao, Heteroepitaxial growth of TiN thin films on Si substrates for MEMS applications, Journal of Alloys and Compounds, 658 (2016) 862-866.

[12] S. Vepřek, P. Nesládek, A. Niederhofer, F. Glatz, M. Jílek, M. Šíma, Recent progress in the superhard nanocrystalline composites: towards their industrialization and understanding of the origin of the superhardness, Surface and Coatings Technology, 108–109 (1998) 138-147.

[13] J.E. Sheehan, K.W. Buesking, B.J. Sullivan, Carbon-carbon composites, Annual Review of Materials Science, 24 (1994) 19-44.

[14] D.J. Kong, H.Y. Guo, Analysis of structure and bonding strength of TiAlN coatings by cathodic ion plating, Materials Science and Processing, 119 (2015) 309-315.

[15] V.Z. Shemet, A.D. Pomytkin, V.S. Neshor, High-temperature oxidation behavior of carbon materials in air, Carbon, 31 (1993) 1-6.

[16] H.B. Jiang, L. Gao, J.G. Li, Preparation of nanocrystalline TiN film by direct nitridation of TiO2 film, Journal of Inorganic Materials, 18 (2003) 495-499.

[17] L. Gu, J. Huang, Y. Tang, C. Xie, S. Gao, Influence of different post treatments on microstructure and properties of WC-Co cemented carbides, Journal of Alloys and Compounds, 620 (2015) 116-119.

[18] C. Liu, N. Lin, Y. He, C. Wu, Y. Jiang, The effects of micron WC contents on the microstructure and mechanical properties of ultrafine WC–(micron WC–Co) cemented carbides, Journal of Alloys and Compounds, 594 (2014) 76-81.

[19] W.C. Lai, Y.-S. Wu, H.-C. Chang, Y.-H. Lee, Enhancing the adhesion of diamond films on cobalt-cemented tungsten carbide substrate using tungsten particles via MPCVD system, Journal of Alloys and Compounds, 509 (2011) 4433-4438.

[20] B. Tian, W. Yue, C. Wang, J. Liu, Surface properties of W-implanted TiN coatings post-treated by low temperature ion sulfurization, Applied Surface Science, 353 (2015) 1156-1163.

[21] A. Leyland, A. Matthews, On the significance of the H/E ratio in wear control: a nanocomposite coating approach to optimised tribological behaviour, Wear, 246 (2000) 1-11.

[22] J. Musil, Hard and superhard nanocomposite coatings, Surface & Coatings Technology, 125 (2000) 322-330.

[23] N. Vidakis, A. Antoniadis, N. Bilalis, The VDI 3198 indentation test evaluation of a reliable qualitative control for layered compounds, Journal of Materials Processing Technology, s 143–144 (2003) 481-485.

Table1 Experimental process parameters

Experimental parameters	Set value
Base pressure	3×10^{-3} Pa
Deposition pressure	0.4 Pa
Substrate cleaning	120 V x 900 s, 300 V x 900 s
Power supply on target	9 A x 4, 50 KHz, 80 %
Filament bias	120 V
Filament discharge current	(6/9/12) A x 3
Gas flow	Ar 120 sccm, N_2 65 sccm
Coating time/h	5

Note: one of the four filaments did not work during the experiments and therefore, the

discharge currents were times by 3.

Table 2 The performance of TiN coatings on 316L austenitic stainless steel and YG8 cemented

carbide

substrate	I_f / A	d /nm	Adhesion /N	Friction coefficient	H /GPa	E /GPa	H/E*	H^3/E^{*2}
316L					6	200	0.028	0.005
TiN on 316L	6	90	87	0.82	8	200	0.038	0.011
	9	49	26.6	0.76	35	450	0.073	0.186
	12	21	21.7	0.65	38	500	0.071	0.192
YG8					25	600	0.04	0.04
TiN on YG8	6	90	141	0.60	8	200	0.038	0.011
	9	49	200	0.79	35	450	0.073	0.186
	12	21	200	0.85	38	500	0.071	0.192

I_f, filament discharge current; d, crystal size; H, nano-hardness; E, Young's modulus;

$$E^* = E/(1-\nu^2), \quad \nu = 0.25$$
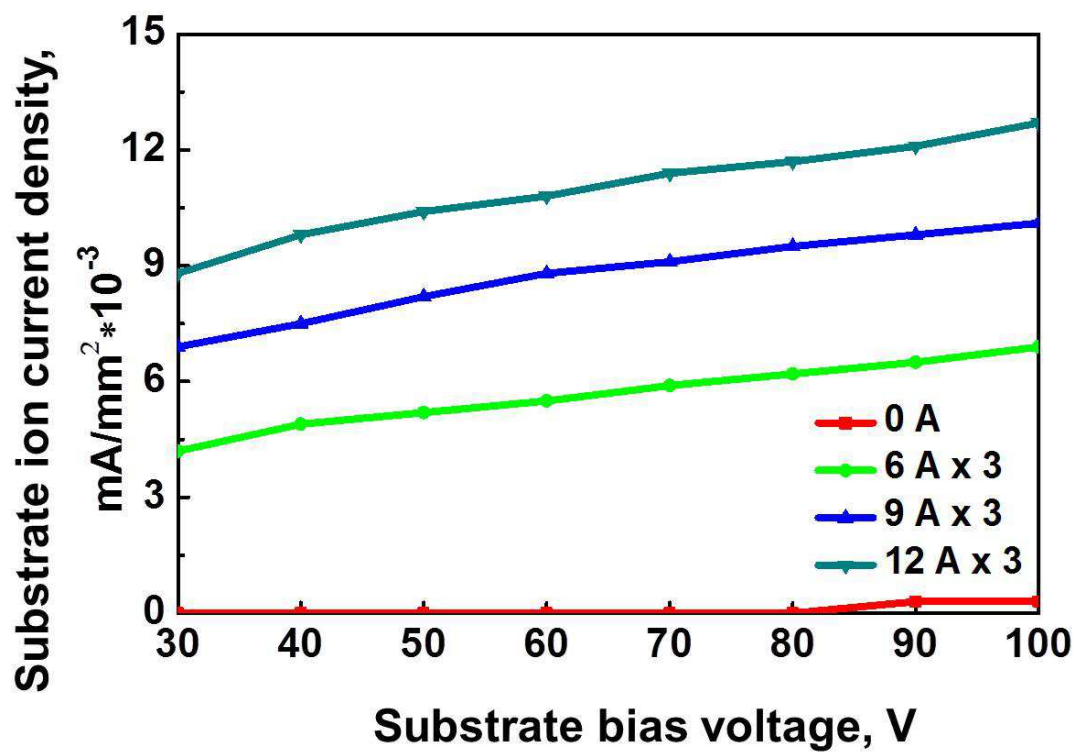
Fig 1
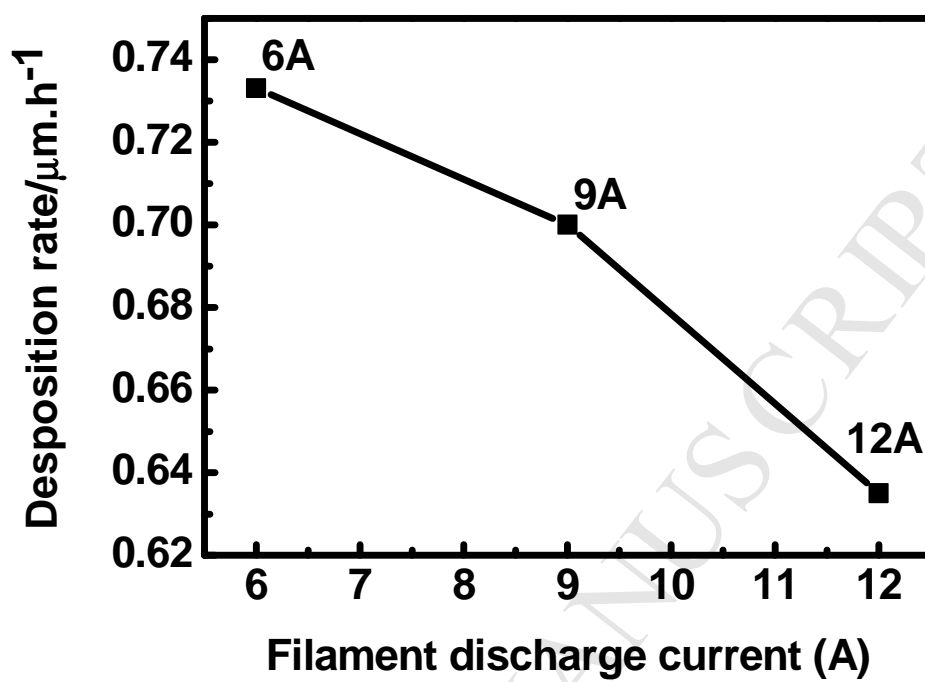
Fig. 2
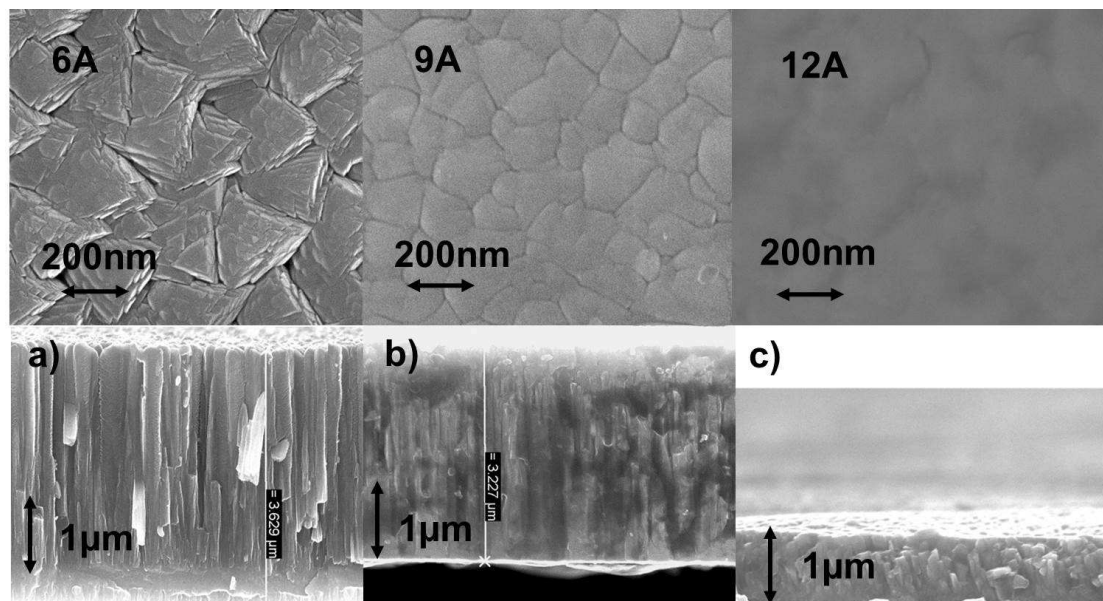
Fig. 3
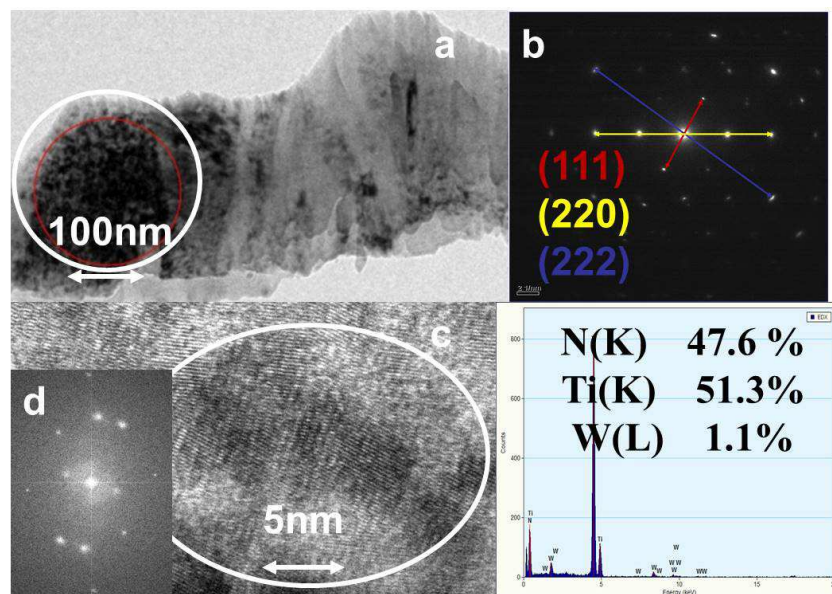
Fig. 4
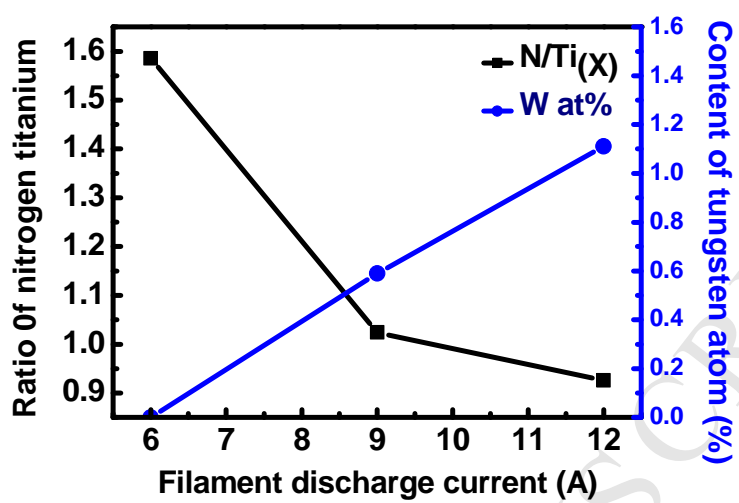
Fig. 5

Fig.6
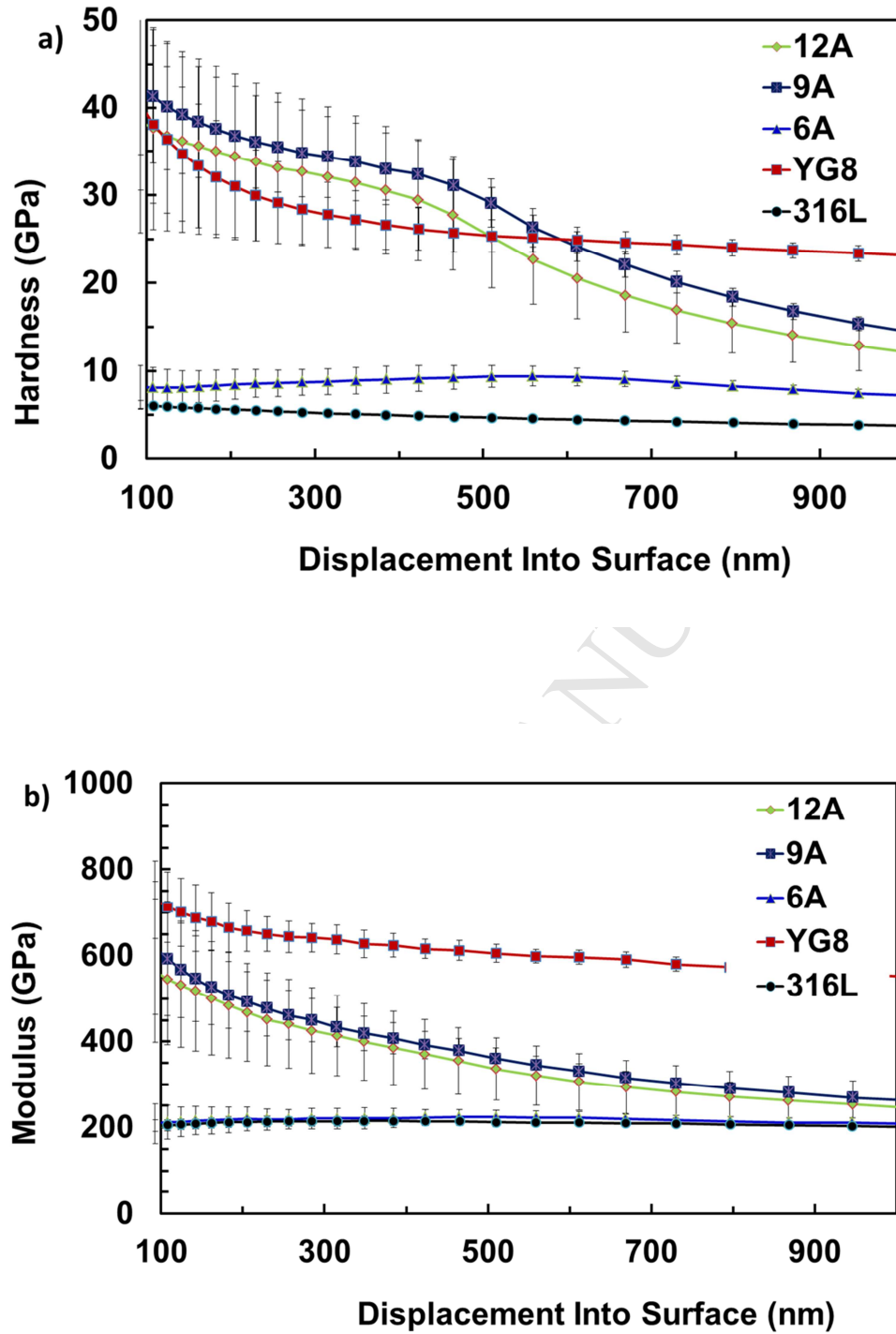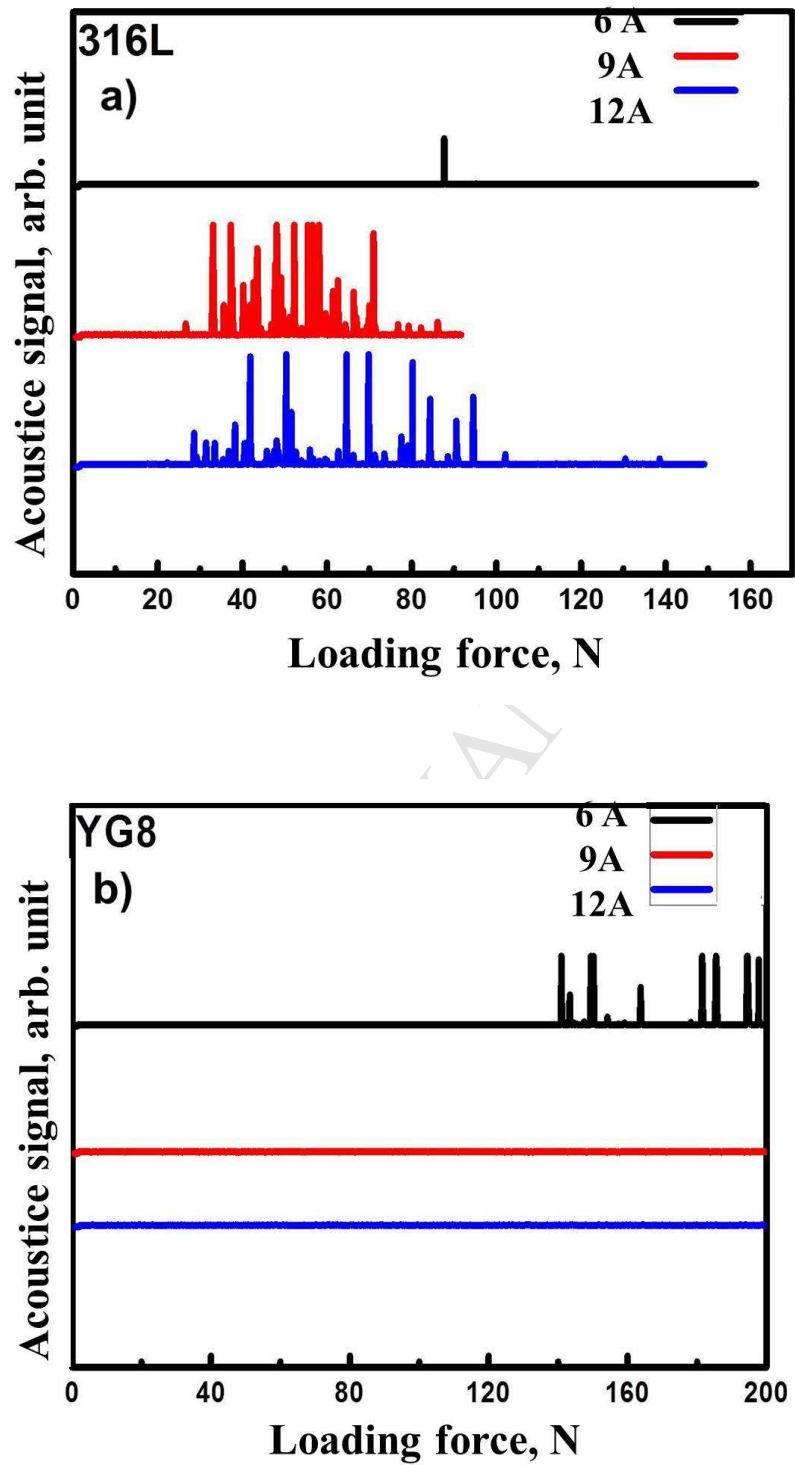
Fig 7

Fig 8

a

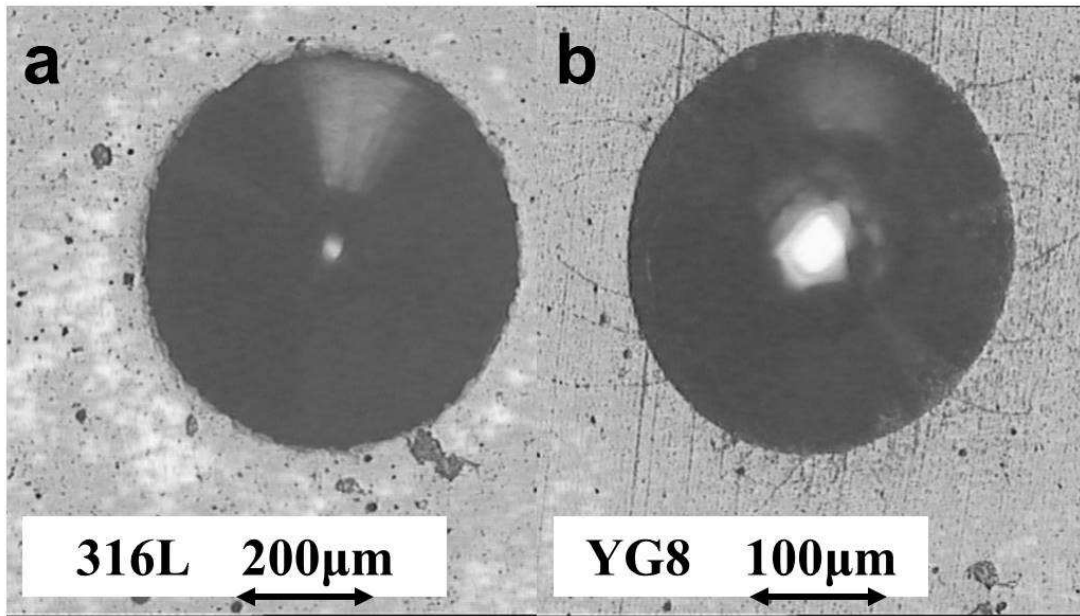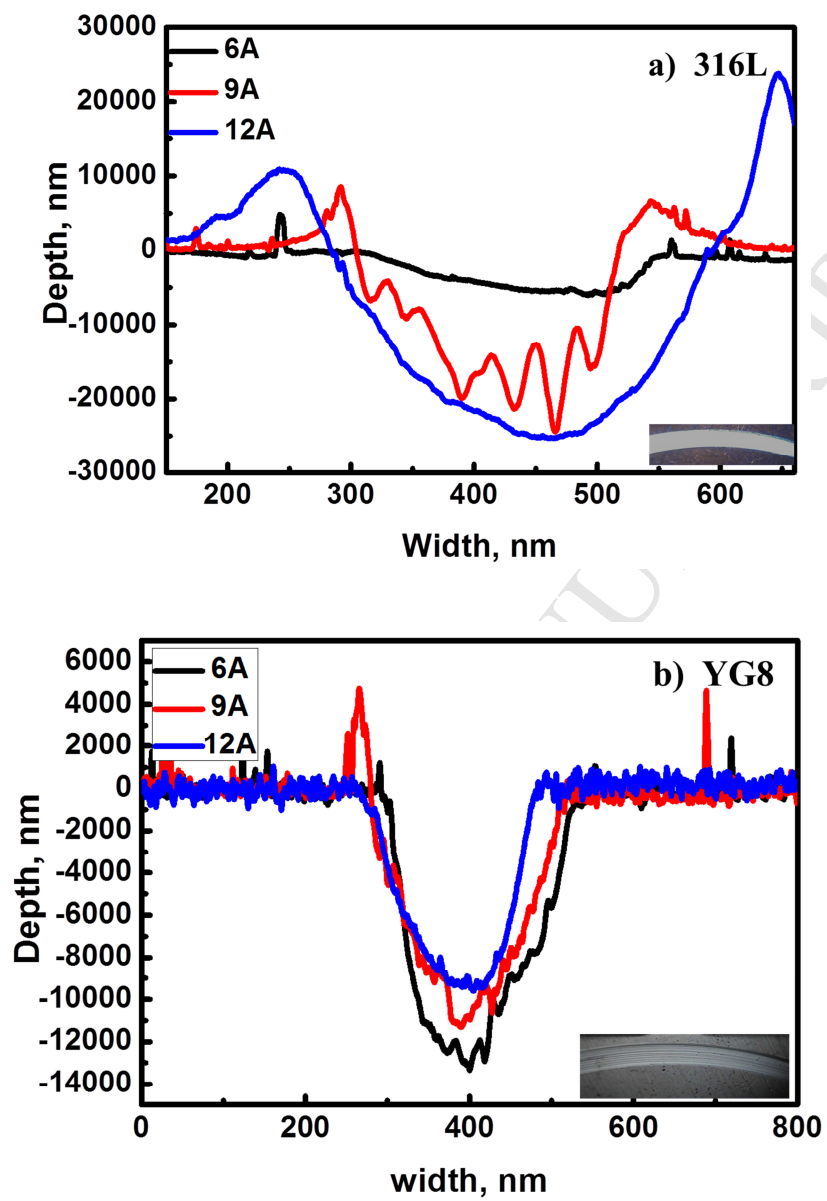316L   200μm

b

YG8   100μm
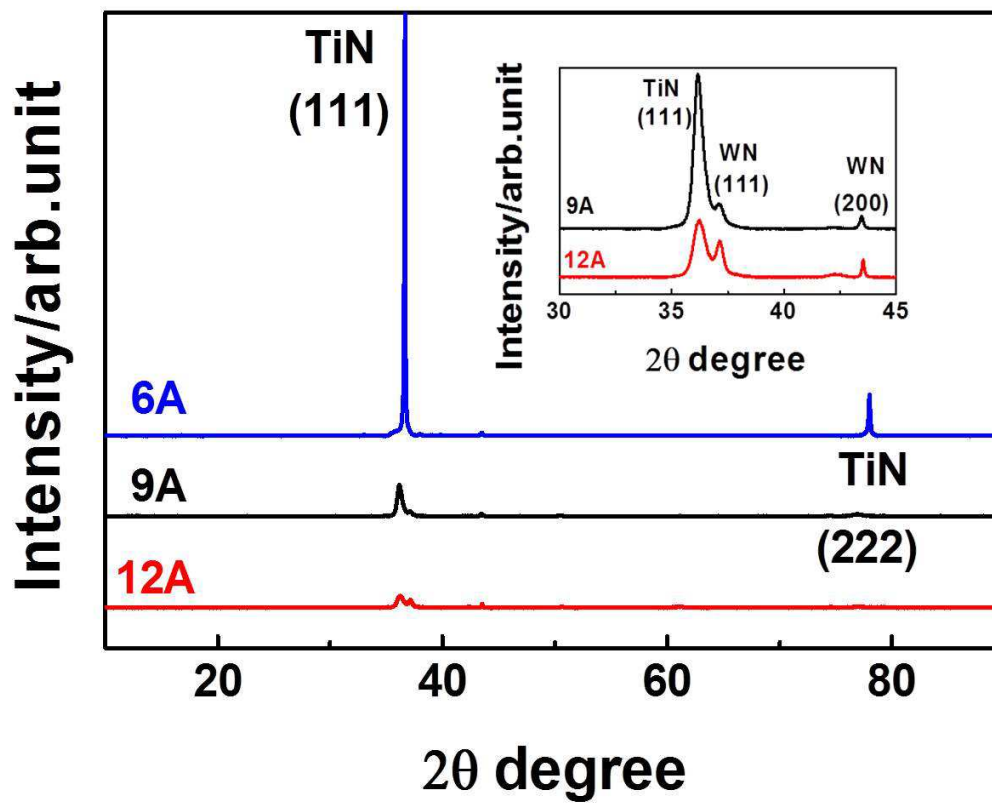
Fig. 6

Fig. 7

Highlights

1. The TiN coating can be compact prepared by hot filament PEMS.

2. The WN phase refined the crystalline and enhanced the hardness.

3. The mechanical performance improved with increasing filament discharge current.

4. The abrasive resistance of TiN coating was affected by substrate's modulus.

5. The adhesion of TiN coating to substrate depended on substrate's modulus.